Neuron
Article

Aversion to Nicotine Is Regulated by the Balanced Activity of β4 and α5 Nicotinic Receptor Subunits in the Medial Habenula

Silke Frahm,[1] Marta A. Ślimak,[1] Leiron Ferrarese,[1] Julio Santos-Torres,[1] Beatriz Antolin-Fontes,[1] Sebastian Auer,[1] Sergey Filkin,[3] Stéphanie Pons,[5] Jean-Fred Fontaine,[2] Victor Tsetlin,[3] Uwe Maskos,[4,5] and Inés Ibañez-Tallon[1,*]
[1]Molecular Neurobiology Group
[2]Computational Biology and Data Mining Group
Max-Delbrück-Centrum, Robert-Rössle-Strasse 10, 13125 Berlin, Germany
[3]Shemyakin-Ovchinnikov Institute of Bioorganic Chemistry, Russian Academy of Sciences, Moscow 117997, Russia
[4]Institut Pasteur, Unité Neurobiologie Intégrative des Systèmes Cholinergiques, Département de Neuroscience, F-75724 Paris cedex 15, France
[5]CNRS, URA2182, F-75724 Paris cedex 15, France
*Correspondence: ibanezi@mdc-berlin.de
DOI 10.1016/j.neuron.2011.04.013

SUMMARY

Nicotine dependence is linked to single nucleotide polymorphisms in the *CHRNB4-CHRNA3-CHRNA5* gene cluster encoding the α3β4α5 nicotinic acetylcholine receptor (nAChR). Here we show that the β4 subunit is rate limiting for receptor activity, and that current increase by β4 is maximally competed by one of the most frequent variants associated with tobacco usage (D398N in α5). We identify a β4-specific residue (S435), mapping to the intracellular vestibule of the α3β4α5 receptor in close proximity to α5 D398N, that is essential for its ability to increase currents. Transgenic mice with targeted overexpression of *Chrnb4* to endogenous sites display a strong aversion to nicotine that can be reversed by viral-mediated expression of the α5 D398N variant in the medial habenula (MHb). Thus, this study both provides insights into α3β4α5 receptor-mediated mechanisms contributing to nicotine consumption, and identifies the MHb as a critical element in the circuitry controlling nicotine-dependent phenotypes.

INTRODUCTION

Tobacco use is a major public health challenge that leads to millions of preventable deaths every year (http://www.who.int/tobacco/statistics/tobacco_atlas/en/). The principal addictive component of tobacco is the plant alkaloid nicotine, which binds and activates nicotinic acetylcholine receptors (nAChRs) (Dani and Heinemann, 1996). In the mammalian nervous system, eight alpha (α2–α7 and α9–α10) and three beta (β2–β4) subunits assemble into pentameric nAChR combinations with distinctive pharmacological and functional properties (Gotti et al., 2009; McGehee and Role, 1995). Recently, genome-wide association studies (GWAs) have identified genetic variants in the *CHRNB4/A3/A5* gene cluster as risk factors for nicotine dependence and lung cancer (Amos et al., 2010a; Saccone et al., 2009; Thorgeirsson et al., 2008; Weiss et al., 2008). These single nucleotide polymorphisms (SNPs) include noncoding variants across the gene cluster, as well as amino acid substitutions (http://www.ncbi.nlm.nih.gov/snp/). Given that *cis*-regulatory elements within the cluster coordinate transcription of these genes for assembly of α3β4-containing (α3β4*) and α3β4α5 functional nAChRs (Scofield et al., 2010; Xu et al., 2006), the fact that a large number of SNPs map to noncoding segments of the cluster suggests that altered regulation of these genes can contribute to the pathophysiology of tobacco use. Indeed the risk for nicotine dependence seems to stem from at least two separate mechanisms: the variability in the mRNA levels of these genes and functional changes due to nonsynonymous amino acid variants (Lu et al., 2009).

A number of mouse models with gene deletions, point mutations, or strain-specific variants in nAChR subunits have been critical to elucidate the role of the different nAChR combinations in nicotine addiction and withdrawal. For instance, α4β2 nAChRs, accounting for 80% of the high-affinity nicotine binding sites in the brain (Whiting and Lindstrom, 1988), are major contributors to nicotine self-administration, as shown in β2 knockout (KO) mice (Maskos et al., 2005; Picciotto, 1998) and in knockin mice with a gain-of-function mutation of α4 (Tapper et al., 2004). The nAChR β4 subunit is almost always coexpressed with α3, while the auxiliary α5 subunit assembles with the α3β4 combination, but can also be incorporated in α4β2 receptor complexes. The expression of the α3β4* nAChR combination is restricted to a few discrete brain areas, including the medial habenula (MHb) and interpeduncular nucleus (IPN), and to autonomic ganglia (Zoli et al., 1995). α3β4* nAChRs have a lower affinity for nicotine than α4β2 receptors and are likely less desensitized at the nicotine levels found in smokers than α4β2 nAChRs are, suggesting that α3β4* nAChRs could play an important role in tobacco addiction, since they retain their sensitivity to fluctuating nicotine levels in smokers (Rose, 2007). β4 and α5 KO mice show similar phenotypes, including

decreased signs of nicotine withdrawal symptoms (Jackson et al., 2008; Salas et al., 2004, 2009), hypolocomotion, and resistance to nicotine-induced seizures (Kedmi et al., 2004; Salas et al., 2004). It has been more difficult to assess the role of α3* nAChRs because KO mice die within 3 weeks after birth due to severe bladder dysfunction (Xu et al., 1999).

Here we show that α3β4α5 nAChR activity in vitro and in vivo is limited by the level of *Chrnb4* expression, and that the ability of the β4 subunit to increase α3β4α5 currents depends on a single, unique residue (S435). This residue maps to the intracellular vestibule of the nAChR complex adjacent to the rs16969968 SNP in *CHRNA5* (D398N), which is linked to a high risk of nicotine dependence in humans. We present a transgenic mouse model of the *Chrnb4-Chrna3-Chrna5* gene cluster, referred to as Tabac (transgenic a3b4a5 cluster) mice, in which *Chrnb4* overexpression enhances α3β4* nAChR levels, resulting in altered nicotine consumption and nicotine-conditioned place aversion (CPA). Lentiviral-mediated transduction of the MHb of Tabac mice with the D398N *Chrna5* variant reversed the nicotine aversion induced by β4 overexpression. This study provides a mouse model for nicotine dependence, demonstrates a critical role for the MHb in the circuitry controlling nicotine consumption, and elucidates molecular mechanisms contributing to these phenotypes.

RESULTS

The Relative Levels of α5 and β4 Subunits Strongly Affect α3β4α5 nAChR Currents

Recently it has been shown that α5 competes with β4 for association with α4, and that this competition does not occur if β4 is substituted with β2 (Gahring and Rogers, 2010). Given that the *CHRNA5-A3-B4* gene cluster regulates the coexpression of α5, β4, and α3 subunits, and that SNPs in the cluster regulatory regions and nonsynonymous variants such as rs16969968 (corresponding to D398N in *CHRNA5*) associate with nicotine dependence (Bierut, 2010; Bierut et al., 2008; Saccone et al., 2009), we were first interested in determining whether variation of the proportion of α3, β4, and α5 (wild-type [WT] and D398N) subunits influences nicotine-evoked currents. To measure this, we performed electrophysiological recordings in oocytes injected with cRNA transcripts of the different mouse subunits. In these experiments (Figure 1), the cRNA concentration of α3 was held constant (1 ng/oocyte), whereas the concentration of β4 or β2 input cRNA was varied among 1, 2, 3, 4, 5, or 10 ng. These experiments showed that β4, but not β2, was able to increase current amplitudes in a dose-dependent manner (Figures 1A and 1B). β4 overexpression did not shift the dose response curves for nicotine (Figure S1A, available online). Next we held constant the concentrations of α3 and β4 at 1:10 and added the cRNA of α5 WT or α5 D397N variant (corresponding to the human α5 variant D398N) at ratios of 1:10:1, 1:10:5, and 1:10:10 (Figure 1A). We observed a significant decrease of current amplitudes at higher concentrations of α5, and this effect was significantly more pronounced with α5 D397N. These results suggest that α5 and β4 may compete for binding to α3, in line with the studies showing such competition for binding to α4 (Gahring and Rogers, 2010).

Given that overexpression of β2 with either α3 (Figure 1A) or α4 (Figure S1B) did not increase currents, we were interested in identifying the residues differing between β4 and β2 that mediate this effect. Since the long cytoplasmic loop is the most divergent domain between nAChR subunits (Figure S1C), and since it has been implicated in cell-surface expression and trafficking of β2 subunits (Nashmi et al., 2003; Ren et al., 2005), we generated β2–β4 chimeras exchanging either this domain, or short motifs and single residues within this domain. Replacement of the cytoplasmic loop of β2 with the corresponding sequences present in β4 (β2/β4 322–496) led to strong increase of nicotinic currents (Figure 1C). Introduction of two β4-specific motifs (a serine/tyrosine rich motif [β2/+β4 382–391] and gephyrin-like-binding motif [β2/+β4 401–419] into the β2 loop) had no influence on current amplitudes (Figure 1C). We next performed bioinformatic analyses and singled out eight β4-specific residues (indicated as T-1 to T-8 in Figure S1C) present within highly conserved motifs. Six of these residues were not further considered: T-2, T-3, T-6, and T-7 residues differ between mouse and chicken β4 subunits, which are equally potent in enhancing nicotine-evoked currents (Figure S1B); T-4 residue lies within the tested motif in the β2/+β4 382–391 chimera; and residues at position T-8 have the same charge (Figure S1C). The remaining two candidates, T-1 (S324 in β4 and T327 in β2) and T-7 (S435 in β4 and R431 in β2) (Figure S1C) were tested by point mutagenesis in the β2 subunit backbone. The β2 T327S point mutant did not increase current, whereas replacement of β2 R431 with serine resulted in a 3.5-fold current increase (Figure 1C). Furthermore, point mutation of the native S435 in the β4 subunit to the arginine residue present in β2 (β4 S435R) abolished the β4-specific activity. Thus, these data demonstrate that the distinctive ability of β4 to increase currents when overexpressed maps to a single residue (S435) that is required in β4 for current increase and can confer this property to β2.

Electrostatic Mapping of the Intracellular Vestibule of the α3β4α5 nAChR Complex

Alignment of mouse, human, and *Torpedo* nAChR subunit sequences indicated that S435 in β4 and D397N in α5 are located in the 25 amino-acid-long amphipathic membrane-associated stretch (MA-stretch) described in the *Torpedo* subunits (Unwin, 2005) (Figure 2A). Electron microscopy studies of the *Torpedo* nAChR have proposed a 3D density map of the receptor complex. In particular, these analyses predict that the MA-stretch of each subunit forms a curved α-helix that helps create, with other α-helices, an inverted pentagonal cone vestibule. To locate the S435 (β4) and D397 (α5) residues within the receptor pentamer, we performed homology modeling with the *Torpedo* nAChR using one possible α3β4α5 subunit arrangement. This model predicted the formation of a very similar disposition of α helices in the α3β4α5 and mapped both residues to the intracellular vestibule (Figure 2B). Electrostatic mapping of the vestibule showed a particular disposition of charges with S435 and D397 located at the more distal and positively charged part of the vestibule (Figure 2C). These data indicate first that the critical residue in β4 that mediates the β4 effect is located in the receptor structure near the most common SNP

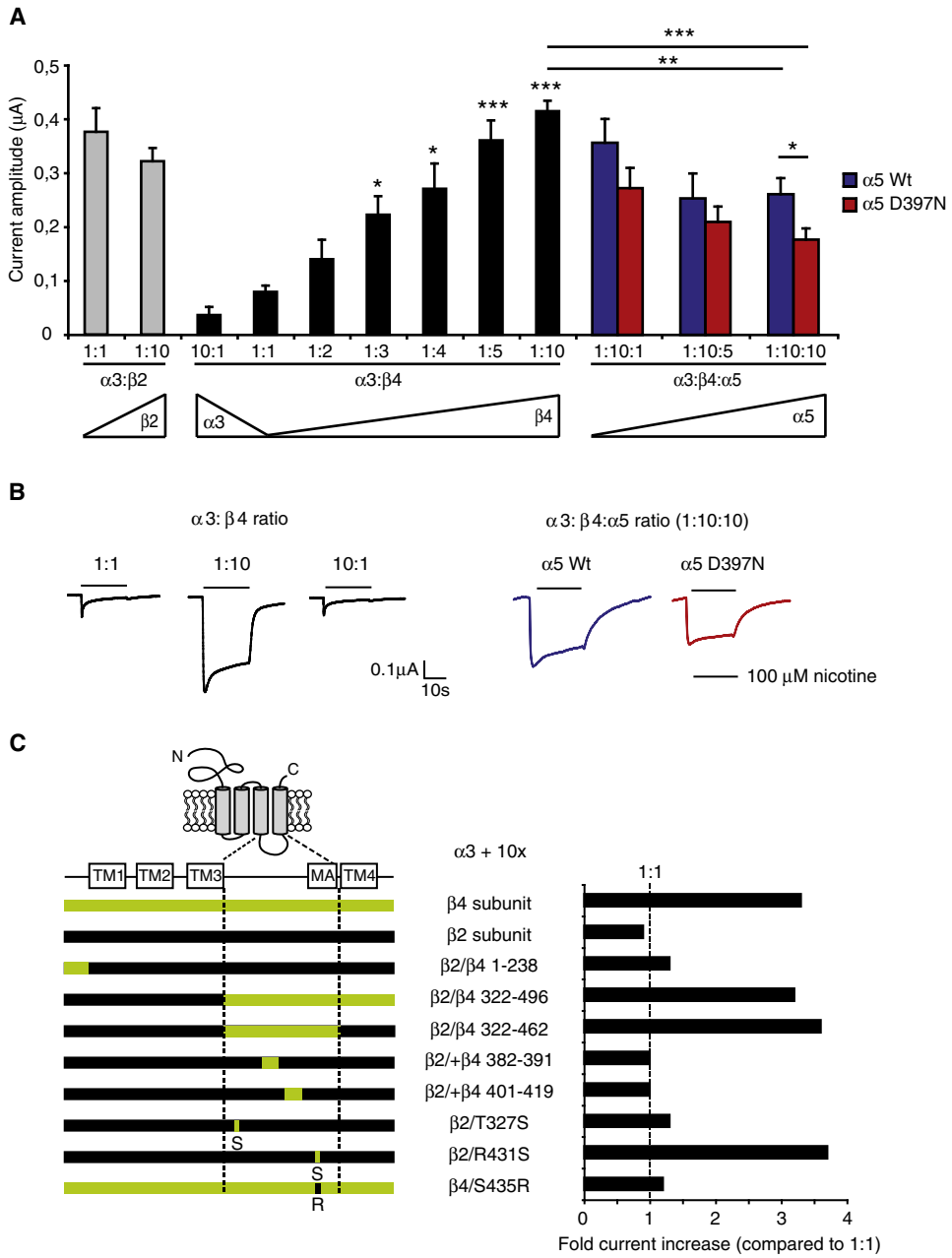

Figure 1. Increase of nAChR Currents by β4 Is Competed by α5 and Maps to a Single Amino Acid (S435)

(A) Quantification of nicotine-evoked currents (100 μM, 20 s) recorded in *Xenopus* oocytes injected with mouse α3:β2, α3:β4, and α3:β4:α5 cRNAs at the indicated ratios. Current amplitudes from 1:3 to 1:10 α3β4 combinations are significantly increased compared to 1:1 ratio (*$p < 0.05$ and ***$p < 0.001$). Addition of α5 to the α3β4 complex leads to significant decrease of current amplitudes when equal amounts of β4 and α5 are injected (**$p < 0.01$ for WT α5 and ***$p < 0.001$ for α5 D397N). The D397N variant shows significantly stronger competition with β4 compared to WT α5 (*$p < 0.05$). Triangles indicate increasing relative amounts of one specified subunit.

(B) Representative traces of two-electrode voltage-clamp recordings.

(C) Schematic representation of β2/β4 chimeras indicating the domains, motifs, or residues exchanged between β4 (in green) and β2 (in black) subunits and corresponding amino acid number and substitutions (left). Fold current increase (right) indicates the relative current amplitude of nicotine-evoked currents for each β2/β4 chimera expressed with the α3 subunit at 1:10 relative to 1:1. All values are expressed as mean ± SEM; n = 5 per ratio in all experiments.

of α5 to be associated with heavy smoking; and second, that this is a highly charged domain of the receptor where single residue changes may have a particularly strong effect on receptor activity.

Transgenic Mice of the *Chrnb4/a3/a5* Gene Cluster, or Tabac Mice

To test the hypothesis that β4 is rate limiting for nAChR assembly and function in vivo and that overexpression of β4 can strongly

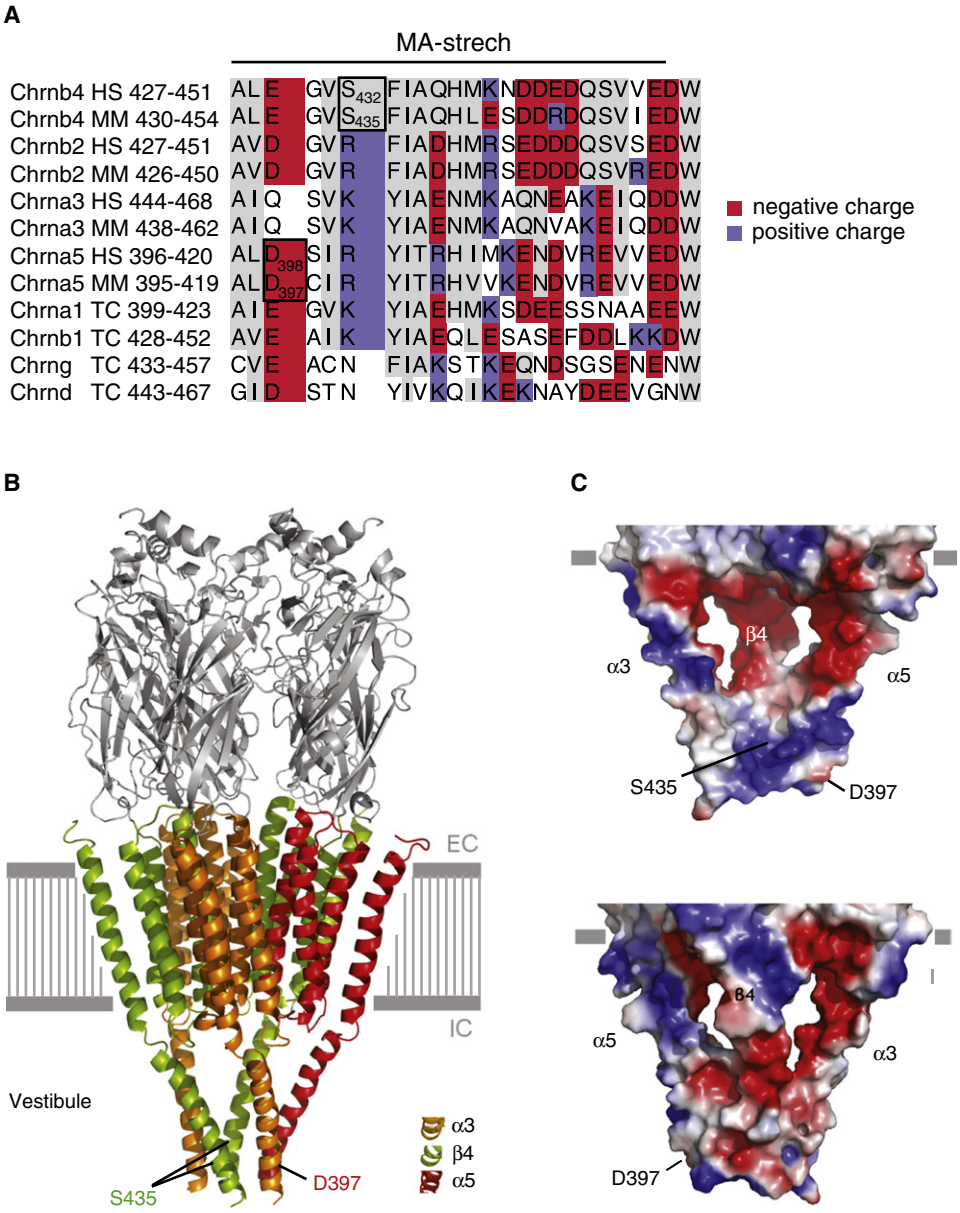

Figure 2. Electrostatic Mapping of the Intracellular Vestibule of the α3β4α5 nAChR Complex

(A) Alignment of human (HS), mouse (MM), and *torpedo* (TC) sequences spanning the MA-stretch of the indicated nAChR subunits. The S435 residue in β4 and the D397 residue in α5 are indicated by a black frame.

(B) Model of the 3D structure of the $\alpha3_2\beta4_2\alpha5_1$ nAChR. Transmembrane and intracellular domains of α3, α5, and β4 subunits are shown in orange, red, and green, respectively. EC, extracellular space; IC, intracellular space. The indicated S435 residue in β4 and the D397 residue in α5 are located at the tip of the intracellular vestibule.

(C) Electrostatic potential surface representations showing frontal (upper panel) and back (lower panel) views of the intracellular vestibule formed by the $\alpha3_2\beta4_2\alpha5_1$ nAChR. One α3 subunit and one β4 subunit are removed for visualization of the cavity. Horizontal gray bars indicate the plasma membrane. The electrostatic surface was contoured between −15kT/e and +15kT/e; negative and positive charges are marked in red and blue, respectively. Residues corresponding to the β4-potentiating residue S435 and D397 in α5 are indicated.

influence nicotine-evoked currents and behavioral responses to nicotine, we characterized a bacterial artificial chromosome (BAC) transgenic line spanning the *Chrnb4-Chrna3-Chrna5* gene cluster (Gong et al., 2003). The BAC transgene included the intact coding sequences of the *Chrnb4* gene, modified sequences of *Chrna3*, and incomplete sequences of *Chrna5. Chrna3* was modified by insertion of an eGFP cassette followed by polyadenylation signals at the ATG translation initiator codon of *Chrna3* (Figure 3A). The upstream sequences of *Chrna5*, encoding exon 1 splice variants (Flora et al., 2000), are missing

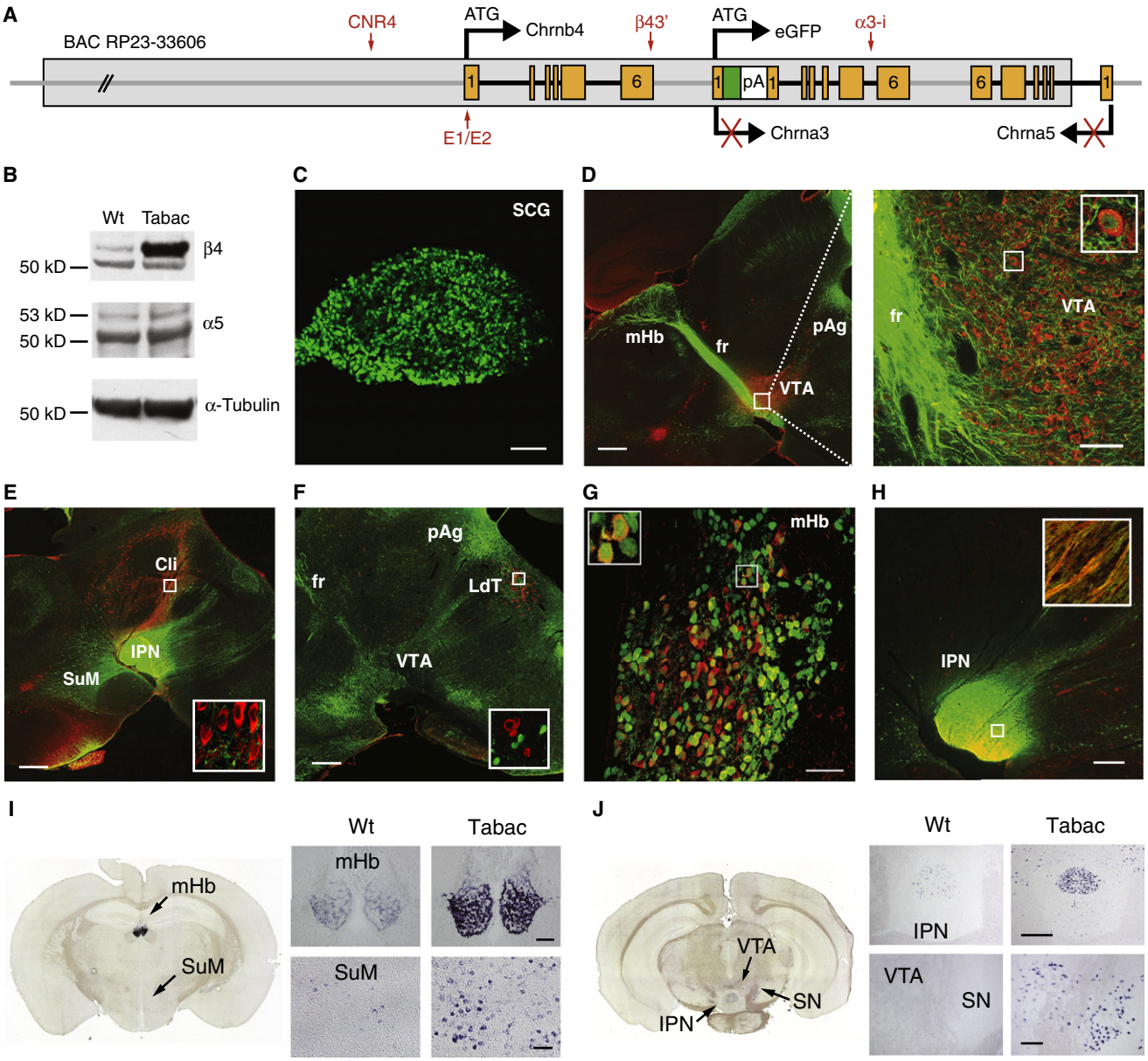

Figure 3. Tabac Mice Express Elevated *Chrnb4* Transcripts in *Chrna3*/eGFP-Labeled Neurons

(A) Scheme of the modified mouse BAC containing the *Chrnb4-Chrna3-Chrna5* gene cluster. Yellow boxes: exons; green box: eGFP cassette; white box: polyadenylation signal (pA); black arrows: direction of transcription; red crosses: truncated transcription; *cis*-regulatory elements marked in red: conserved noncoding region (CNR4), β43′ enhancer (Xu et al., 2006); E1/E2: SP1 and SP3 binding sites (Bigger et al., 1997); and α3-i: transcriptional silencer (Medel and Gardner, 2007).

(B) Western blot analyses of β4 (53 kD), α5 (two splice variants: 50 kD and 53 kD), and α-tubulin in brain extracts of WT and Tabac mice.

(C–H) eGFP-expressing neurons (green) in peripheral SCG (C) and in sagittal brain sections (except G: coronal) of Tabac mice immunostained with TH (D and E) and ChAT (F–H) in red. Scale bars: (C) 100 μm; (D–F) 500 μm (magnification of D is indicated by the dotted lines; scale bar: 50 μm); (G) 50 μm; and (H) 250 μm.

(I and J) ISH of *Chrnb4* transcripts in WT and Tabac brain sections. Scale bars: MHb, 100 μm; SuM, 50 μm; IPN, 250 μm; VTA, 100 μm.

TH, tyrosine hydroxylase; ChAT, choline acetyltransferase; MHb, medial habenula; fr, fasciculus retroflexus; VTA, ventral tegmental area; pAg, periaqueductal gray; Cli, caudal linear nucleus; SuM, supramammilary nucleus; IPN, interpeduncular nucleus; LdT, laterodorsal tegmentum; SN, substantia nigra; SCG, superior cervical ganglia.

in the BAC transgene (Figure 3A). To promote correct expression of *Chrnb4*, the BAC included the intergenic and 5′ flanking regions encompassing the *cis*-regulatory elements that coordinate cotranscriptional control of the genes in the cluster (Bigger et al., 1997; Medel and Gardner, 2007; Xu et al., 2006). As a result of these modifications in the BAC transgene, these Tabac mice express high levels of β4, but not α5 (Figure 3B), and expression of α3 is replaced by expression of an eGFP reporter cassette to

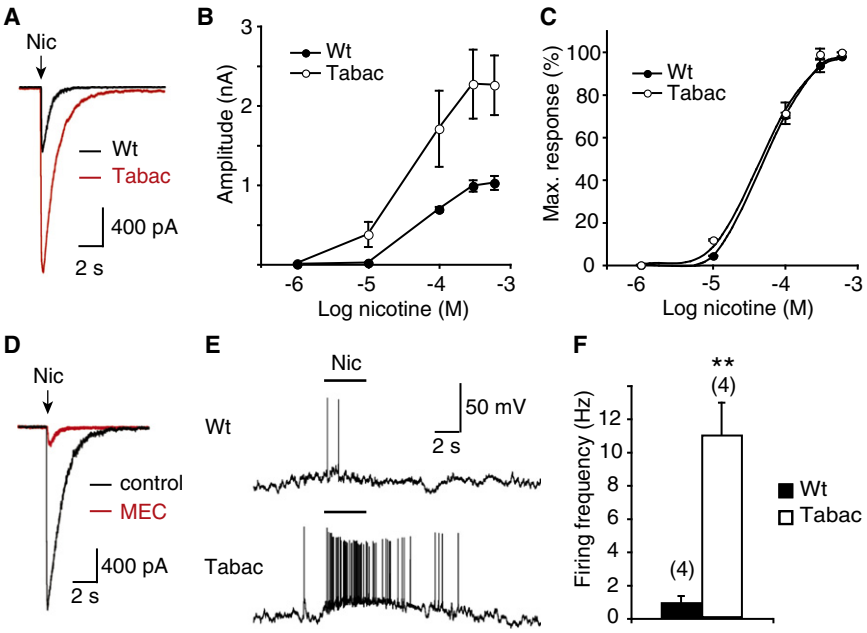

Figure 4. Tabac Mice Show Increased Nicotine-Evoked Currents and Firing Frequency in *Chrna3*/eGFP-Labeled Neurons

(A–F) Whole-cell patch-clamp recordings of MHb neurons in acute brain slices from WT and Tabac mice. Representative traces of nicotine-evoked currents (A: 100 μM, 50 ms application) and corresponding concentration-response relationships (B: peak amplitudes ± SEM, n = 5–8 cells per genotype, $p < 0.05$ by two-way ANOVA). Dose-response curves in (C) were calculated relative to the maximal response to nicotine from (B). (D) Mecamylamine (MEC, 3 μM, 3 min) inhibition of nicotine-evoked currents in neurons of Tabac mice. Representative current clamp recordings (E) and quantification of action potentials upon local application of nicotine (1 μM, 3 s) in neurons of WT and Tabac mice are shown in (F) (mean firing frequency ± SEM, n = 4, $p < 0.01$). Numbers in parenthesis represent number of neurons tested. All values are expressed as mean ± SEM.

monitor the sites expressing the transgene (Figures 3C–3H). As shown in Figure 3, neurons expressing eGFP were evident in autonomic ganglia (Figure 3C), and in very restricted brain structures (Figures 3D–3H) known to express these genes (Zoli et al., 1995). Immunostaining with cholinergic (ChAT) and dopaminergic (TH) markers indicated high expression of *Chrna3*/eGFP in ChAT neurons of the Hb-IPN system (Figures 3G and 3H). Intense *Chrna3*/eGFP expression was also detected in other brain areas (Figures 3D and 3E) involved in nicotine addiction, such as the ventral tegmental area (VTA), the caudal linear nucleus (Cli), the supramammilary nucleus (SuM) (Ikemoto et al., 2006), and the laterodorsal tegmental nucleus (Figure 3F), which provides modulatory input to the VTA (Maskos, 2008). We performed in situ hybridization (ISH) experiments to verify that the BAC accurately directed expression of transgenic *Chrnb4* transcripts to eGFP-positive brain areas. Tabac mice showed a prominent enrichment of *Chrnb4* transcripts in α3β4*-positive areas, such as MHb and IPN, and in brain areas that have been shown to express lower levels of *Chrnb4*, such as SuM (Dineley-Miller and Patrick, 1992) and VTA (Yang et al., 2009) (Figures 3I and 3J). RT-PCR studies showed that *Chrna4*, *Chrna7*, and *Chrnb2* transcripts (which are not present in the BAC) are not altered in Tabac mice (Figure S2). Taken together these data show that Tabac mice express high levels of β4, but not α5, in α3/eGFP-labeled cells in CNS and PNS structures known to express the *Chrnb4-Chrna3-Chrna5* nicotinic gene cluster, and are thus a useful mouse model in which to test the consequences of enhanced β4 expression at endogenous sites.

Increased Nicotine-Evoked Currents in Transgenic Tabac Mice

Given the demonstration that the level of β4 expression is rate limiting for the function of α3β4α5 receptors in vitro (Figure 1), we were next interested in determining whether enhanced expression of *Chrnb4* in Tabac neurons resulted in elevated nicotine-evoked currents in vivo. Previous studies have shown that neurons in the MHb express high levels of α3β4α5 receptors (Quick et al., 1999). Accordingly, we employed patch-clamp recordings to measure nicotine-evoked currents in MHb neurons of Tabac mice. A large proportion of MHb neurons in WT mice (n = 20 of n = 23 neurons recorded) responded to local fast application (50 ms) of nicotine (Figures 4A and 4B). In *Chrna3*/eGFP-labeled MHb neurons of Tabac mice, nicotine elicited significantly increased peak currents in comparison to WT littermates (on average, 3.4-fold at 100 μM nicotine, two-way ANOVA, $p < 0.05$) (Figure 4B). Similarly increased responses were obtained using acetylcholine (ACh) (data not shown). Dose-response curves for nicotine showed no significant differences between WT and Tabac mice, indicating that the affinity of the receptors in the transgenic mice is not altered (Figure 4C). Application of mecamylamine (MEC), a nonselective potent inhibitor of α4β2* and α3β4* nAChRs (Bacher et al., 2009), resulted in a blockade of as much as 90% of the nicotine-elicited responses in Tabac mice (Figure 4D), demonstrating that the enhanced nicotine responses in Tabac neurons result directly from elevated levels of functional nAChRs. To determine whether these additional receptors cause enhanced neuronal excitability, the firing rate of habenular neurons was measured in current-clamp assays in response to nicotine. Neurons from WT and Tabac mice were silent at rest (−70 mV). Local nicotine application (1 μM for 3 s) elicited single action potentials in WT neurons, whereas nicotine induced a robust burst of action potentials with a 13-fold higher firing frequency on average in Tabac neurons ($p < 0.005$) (Figures 4E and 4F). Together, these results indicate that the increased sensitivity of MHb neurons to nicotine in Tabac mice results from the presence of additional functional nAChRs, rather than from changes in the nicotine affinity of existing receptors.

Tabac Mice Have Increased Numbers of α3β4* nAChR Binding Sites

To assay for elevated receptor expression across different brain structures, we performed autoradiographic radioligand binding assays with iodinated epibatidine, which mainly binds α4β2* and α3β4* nAChRs (Perry and Kellar, 1995) (Figures 5A and 5B). Competition with cold cytisine, which binds with higher affinity to α4β2* than to α3β4* receptors (Marks et al., 2010), was done to distinguish α3β4* from overlapping α4β2* binding sites (Zoli et al., 1998) (Figures 5C and 5D). In WT mice, discrete brain regions resistant to cytisine competition labeled well-known α3β4* sites such as MHb, IPN, and superior colliculus (Figure 5C). In Tabac mice, increased radioligand binding to cytisine-resistant sites was detected in these areas and in additional brain structures, including the VTA, SuM, substantia nigra, and striatum (Figure 5D). A strong correlation between radioligand signal and eGFP fluorescence was detected in all analyzed CNS structures (Figure 5E and Table S1). Densitometric analyses indicated significantly increased cytisine-resistant signals in α3β4*-expressing regions in Tabac mice (Table S1), while α4β2* epibatidine binding sites such as cortex and thalamus did not differ between control and Tabac mice (Figures 5A and 5B), indicating that elevated surface receptors are present in sites corresponding to endogenous β4 expression sites. To exclude the possibility that the increased radioligand signal could reflect increased cell number, we quantified the cell density in MHb of Tabac and WT mice and observed no significant differences (Figure S3). These data show that the enhanced nicotine-evoked currents in Tabac mice result from β4-mediated recruitment of additional functional α3β4* nAChR complexes on the cell surface.

Taken together, the anatomic mapping and ISH results presented in Figure 3 and the receptor binding assays presented in Figure 5 provide compelling evidence that α3β4* nAChRs are located both on the cell soma and in the axon termini. For example, the relatively light staining of the IPN by ISH in Tabac mice strongly suggests that the very heavy expression of functional α3β4* receptors, detected in this structure by receptor binding, results from both local synthesis in the IPN and the presence of receptors synthesized in the MHb and transported to presynaptic termini in the IPN. This is consistent with the well-documented effects of presynaptic nAChRs on synaptic release and neurotransmission (McGehee et al., 1995), and suggests that Tabac mice will be an important tool for further dissection of the roles of presynaptically and postsynaptically expressed nAChRs.

Tabac Mice Show a Strong Aversion to Nicotine Consumption and Display Nicotine-CPA

We were next interested in the effects of elevated nAChR expression on the behavioral responses of Tabac mice to nicotine. Measurements of drinking volumes showed that Tabac mice consumed significantly less nicotine-containing-water than WT littermates did (Figures 6A and 6B). Because nicotine solutions have a bitter taste, nicotine was diluted in saccharin solution, and control experiments were performed with a bitter solution (containing quinine). There were no differences in consumption of regular, sweetened, or bitter water between the two groups (Figure 6A). Next, we performed a free choice consumption experiment where mice were allowed to choose between regular water and water supplemented with different concentrations of nicotine (1–100 μg/ml) without saccharin. Analysis of the nicotine volume consumed relative to the total fluid intake (Figure 6C) indicated that Tabac mice significantly avoided drinking nicotine solutions containing more than 5 μg/ml nicotine ($p < 0.05$, two-way ANOVA), while WT mice showed no preference between water and nicotine solutions below 50 μg/ml and avoided drinking the highest concentration of nicotine solution tested. It is possible that the decrease in drinking is due to negative consequences of hyperactivation of the autonomic nervous system, leading to gastric distress or nausea. However, we observed no significant differences in body weight (Figure 6D), micturition, and digestion (Figure S4) before and during the nicotine consumption experiments.

As an independent measure of the effects of nicotine in Tabac mice, CPA assays were performed. Because conditioning to nicotine is both concentration and strain dependent (O'Dell and Khroyan, 2009) we measured CPA in WT C57BL/6 littermates at 0.5 mg nicotine/kg body weight. Under these conditions, we observed neither a preference for nor aversion to nicotine. In contrast, strong CPA to nicotine was observed in Tabac mice (Figure 6E). These data both confirm the conclusions of the nicotine consumption assays, and demonstrate that negative reward learning associated with nicotine is strongly increased in Tabac mice. We conclude that overexpression of the β4 subunit in vivo leads to an increase in functional α3β4* receptors, resulting in a higher sensitivity to the aversive properties of nicotine.

Lentiviral-Mediated Expression of the α5 D397N Variant in the MHb Reverses Nicotine Aversion in Tabac Mice

The observations that the α5 D397N variant reduces α3β4α5 nicotine-evoked currents in oocytes (Figure 1), and that the MHb-IPN tract contains a high density of native α5 nAChR subunits in combination with α3β4 subunits (Figure 3), suggested that the enhanced nicotine aversion evident in Tabac mice could be reversed by expression of the α5 variant in the MHb. To test this hypothesis we employed lentiviral-mediated transduction to express the α5 D397N in MHb neurons of Tabac mice. We injected bilaterally either control lentivirus (LV-PC) or the LV-α5 D397N (LV-α5N) viruses in Tabac mice. As shown in Figure 7B, immunostaining for the mCherry reporter of LV-α5N expression or direct fluorescence derived from the control lentivirus demonstrated that the lentiviral-transduced area corresponds with that occupied by α3β4*/eGFP-labeled neurons in the MHb of Tabac mice. Given that the maximal difference in nicotine consumption in Tabac mice occurred at 25 μg/ml nicotine (Figure 6C), mice were again given a two-bottle choice test to measure nicotine aversion. These experiments were performed in Tabac mice backcrossed to the inbred mouse line C57BL/6 (Figure 7C), which has been shown to have a high basal level of self-selection of nicotine (Glatt et al., 2009; Meliska et al., 1995; Robinson et al., 1996), and in Tabac mice outbred between FBV/N mixed and Swiss Webster (Figure 7D). As shown in Figure 7C, in C57BL/6 Tabac mice, injection of the LV-α5N virus reversed their nicotine aversion in comparison to mice injected with the control virus. In outbred Tabac mice injected with the control virus, we observed

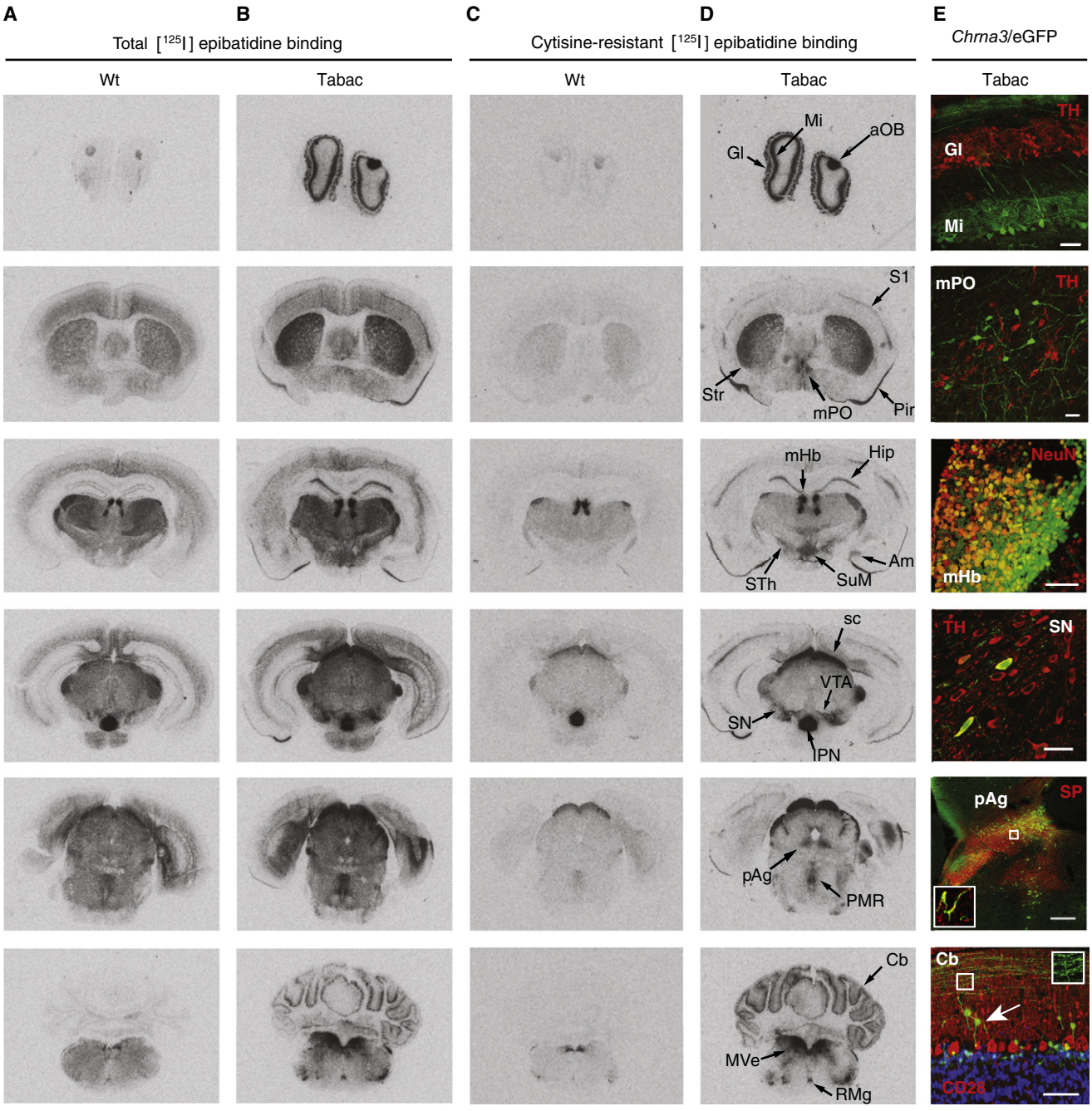

Figure 5. Increased Number of α3β4* nAChR Binding Sites in Tabac Mice

(A and B) Film autoradiograms of [^{125}I]-epibatidine binding to α3β4* and α4β2* sites in WT (A) and Tabac (B) coronal brain sections.

(C and D) Detection of α3β4* sites (arrows) by competition of [^{125}I]-epibatidine binding with unlabeled cytisine.

(E) Direct fluorescence (green) of *Chrna3*/eGFP-positive cell populations and immunostaining of coronal brain sections from Tabac mice with the indicated antibodies (red: TH, NeuN, Substance P [SP], and CD28). Scale bars from top to bottom are 50, 25, 50, 25, 250, and 50 μm.

Mi, mitral cells; Gl, granule layer; aOB, accessory olfactory bulb; mPO, medial preoptic area; S1, primary sensory cortex layer IV; Pir, piriform cortex; Hip, hippocampus; Am, amygdala; STh, subthalamic nucleus; sc, superior colliculus; PMR, paramedian raphe nucleus; Cb, cerebellum; arrow, basket cells; insert, parallel fibers; RMg, nucleus raphe magnus; and MVe, medial vestibular nucleus Other abbreviations are the same as in Figure 1.

no alteration in nicotine aversion (Figure 7D) with respect to uninjected Tabac mice (Figure 6C). Importantly, infection with LV-α5N virus reversed nicotine aversion in Tabac mice (Figure 7D), restoring nicotine consumption in α5 D397N-infected Tabac mice to levels evident in WT mice (Figure 6C). These results demonstrate a major role for the MHb in nicotine consumption.

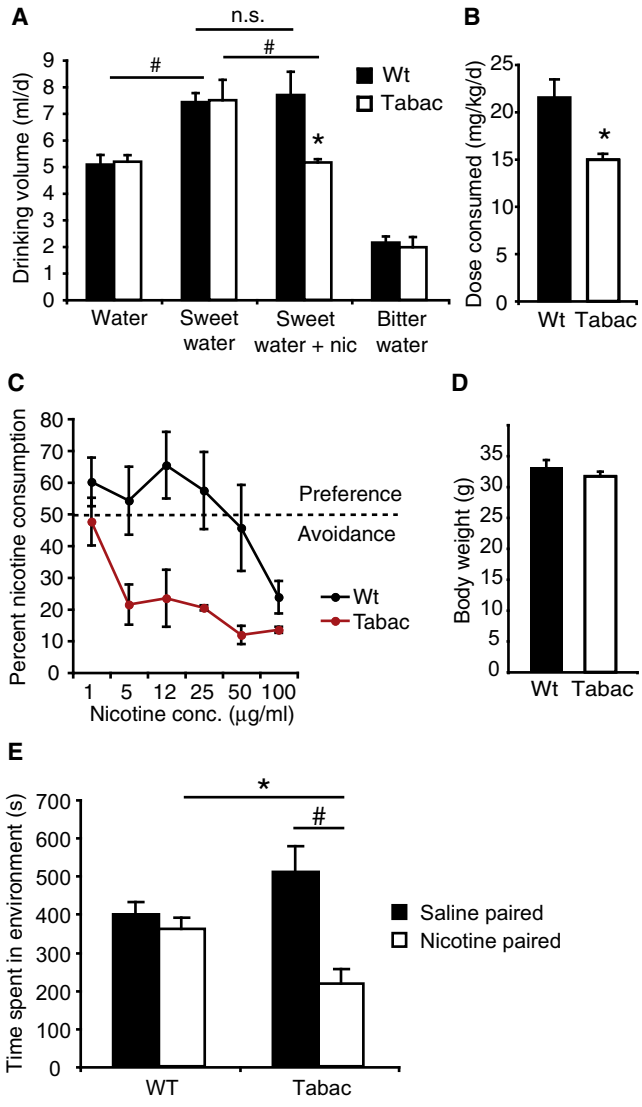

Figure 6. Tabac Mice Consume Less Nicotine and Show Conditioned Place Aversion

(A and B) Nicotine consumption in a no-choice paradigm (one drinking bottle). (A) Drinking volumes (ml/mouse/day) of water, sweet water (2% saccharine), and bitter water (5 mM quinine). The tested period of consumption was 3 days (paired t test, #$p < 0.05$). (B) The dose of nicotine consumed expressed as the milligrams of nicotine consumed per day considering the body weight of the mouse (mg/kg/d) ($p < 0.05$). WT: n = 10, Tabac: n = 10.

(C) Nicotine consumption in a two-bottle choice paradigm between water and water containing the indicated nicotine concentrations expressed as percent of the volume of nicotine solution consumed divided by the total fluid intake per day. Each concentration was tested for 3 days. Dashed line at 50% indicates no preference. WT mice, n = 7; Tabac mice, n = 6; two-way ANOVA, $p < 0.05$.

(D) Body weight of WT and Tabac mice after nicotine drinking tests.

(E) Nicotine administration (0.5 mg/kg) elicits place aversion to a nicotine-paired environment in Tabac mice. Following conditioning, Tabac mice preferred the saline-paired environment over the nicotine-paired environment (paired t test, #$p < 0.05$). WT mice spent significantly more time in the nicotine-paired environement compared to Tabac mice (*$p < 0.05$) (WT mice, n = 7; Tabac mice, n = 6). Data are expressed as time spent in drug-paired environments after drug conditioning. All values are expressed as mean ± SEM.

DISCUSSION

Human genetic studies have established an association between the *CHRNB4-CHRNA3-CHRNA5* locus and tobacco use (Amos et al., 2010b; Saccone et al., 2009; Thorgeirsson et al., 2008; Weiss et al., 2008). Here we report a mouse model (Tabac mice) with altered nicotine consumption and CPA caused by elevated levels of β4, enhanced nicotine-evoked currents, and increased surface expression of functional nAChRs at endogenous sites. The ability of β4 to enhance nicotine-evoked currents depends on a single critical residue (S435) located in the intracellular vestibule of the receptor. Interestingly, modeling studies revealed that one of the most common SNPs associated with tobacco usage, D398N in the α5 subunit, also maps to this domain. Functional analyses of this variant demonstrate that alterations in this domain can result in profound effects on nicotine-evoked currents. Based on our studies in Tabac mice in which enhanced current is associated with increased aversion to nicotine, we predicted that the α5 variant (corresponding to D397N in mice) should increase nicotine consumption consistent with its association with smoking. To test this idea, and given that the MHb contains a very high concentration of endogenous α3β4α5 receptors and elevated levels of β4 driven by the Tabac transgene, we introduced the α5 variant by viral-mediated transduction in habenular neurons of Tabac mice. The reversal of the nicotine aversion achieved in Tabac mice observed in these experiments demonstrates that the MHb plays a major regulatory role in nicotine consumption.

Three main points are addressed in this study. First, changes both in the coordinated expression of α3β4α5 subunits (i.e., overexpression of the β4 subunit) and in single residues (i.e., in vivo viral-mediated expression of the α5 D397N variant) have a strong influence on nicotine consumption in mice. This is consistent with recent GWAs that have identified SNPs in both regulatory and coding regions of the *CHRNB4-CHRNA3-CHRNA5* gene cluster that are associated with nicotine dependence (Levitin et al., 2008; Saccone et al., 2009; Thorgeirsson et al., 2008). Thus, our studies provide a model for further exploration of the involvement of α3β4α5 nAChR function in nicotine consumption. Second, our studies demonstrate that the intracellular vestibule of the α3β4α5 receptor exerts an important effect on nicotine-evoked currents. The high concentration of charges in this membrane-associated domain is conserved in the superfamily of Cys-loop receptors (Carland et al., 2009; Kelley et al., 2003; Unwin, 2005). Electrostatic calculations by homology with the *Torpedo* nAChR predict that α3β4α5 receptors form a highly electronegative vestibule most likely to promote a stabilizing environment for cation outflow. The change in current amplitude produced by substitutions of charged residues (S435R and D397N) in this domain of the receptor predicts that alterations of the electrostatic charge of the vestibule are critical for receptor function. This is consistent with studies of the inner vestibule in other Cys-loop receptor channels. For example, in 5HT3A receptors substitution of arginine-positive residues increased channel conductance, whereas introduction of basic residues in this domain of α1 glycine receptors decreases glycine-evoked currents (Carland et al., 2009; Kelley et al., 2003). Numerous reports have linked the α5 D398N polymorphism to

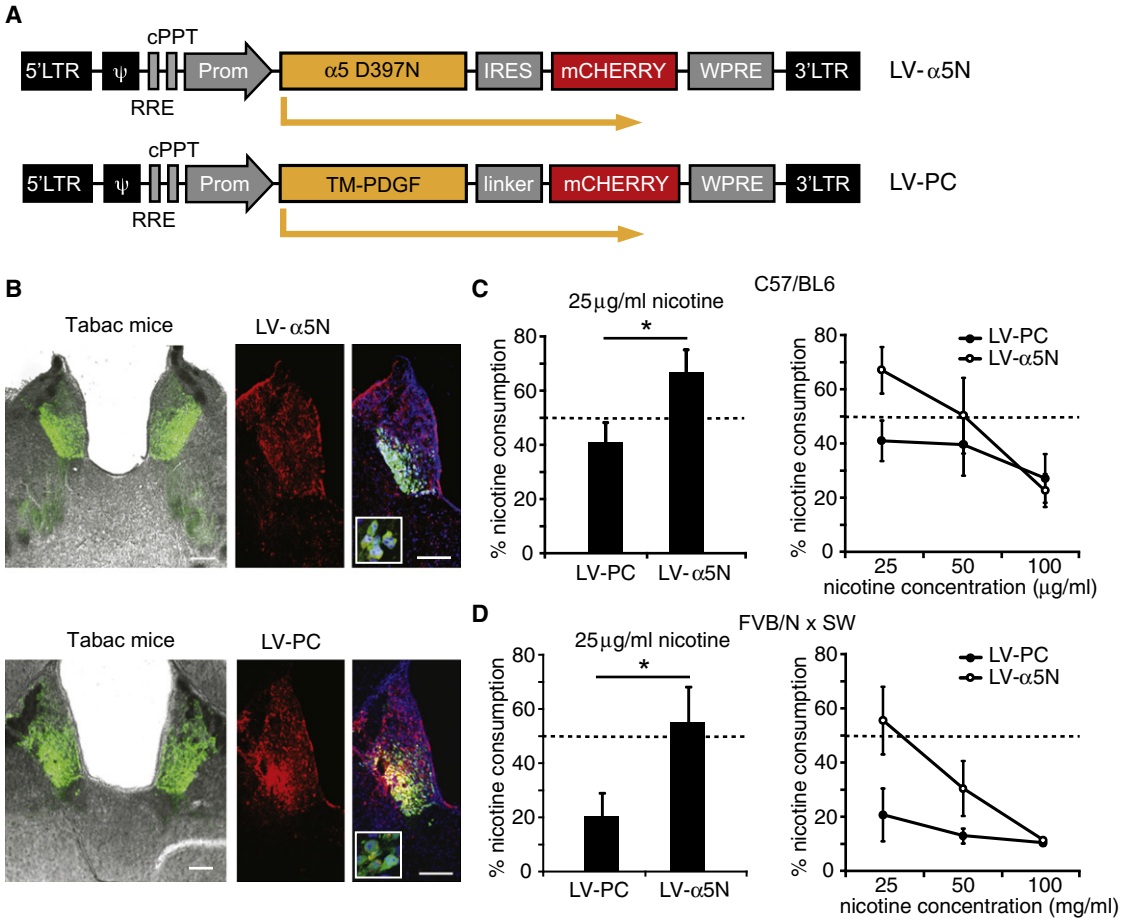

Figure 7. Reversal of Nicotine Aversion in Tabac Mice by Lentiviral-Mediated Expression of the α5 D397N Variant in the MHb

(A) Schematic representation of the lentiviral (LV) constructs used for brain stereotactic injections. LV-α5N carries the mouse α5 variant D397N followed by an IRES and the mCherry reporter. The control virus (LV-PC) carries mCherry fused to the N terminus of the transmembrane domain of the PDGF receptor (TM-PDGF) via a linker domain.

(B) Coronal brain sections of Tabac mice stereotactically injected in the MHb with the indicated lentivirus. Colocalization of eGFP fluorescence driven by the transgene in Tabac mice and mCherry red fluorescence for LV-PC or mCherry immnofluorescence for LV-α5N injected mice is shown. Scale bars: 100 μm.

(C and D) Two-bottle choice nicotine consumption in Tabac mice after stereotactic bilateral injection of control (LV-PC) and mutated α5 (LV-α5N) lentiviral constructs in the MHb. Tabac mice were backcrossed to C57BL/6; n = 4 for LV-PC and n = 5 for LV-α5N, $p < 0.05$ (C), and Tabac mouse hybrid of FVB/N and Swiss Webster (n = 8 for LV-PC and n = 9 for LV-α5N) is shown in (D).

All values expressed are mean ± SEM.

smoking incidence (Bierut, 2010; Bierut et al., 2008; Saccone et al., 2009). Incorporation of D398N α5 variant into α4β2-containing receptors in transfected cells results in a 2-fold reduction in epibatidine-evoked calcium currents without a change in surface expression (Bierut et al., 2008), consistent with the reduction in nicotine-evoked current amplitudes reported here upon incorporation of this variant into α3β4-containing nAChRs. Taken together, these observations support the hypothesis that substitution of this charged residue modifies the vestibule electrostatic charge, but not the number of receptors incorporated into the plasma membrane. In contrast, the increase in receptor surface expression in Tabac mice and the identification of a single residue in the β4 subunit (S435R) that is both essential for the increase of currents observed in this study upon overexpression of the β4 subunit, and that can confer this property upon β2 subunits, suggest that the β4 subunit is rate limiting for the formation of α3β4α5 nAChRs. Although the precise role of S435 is not yet clear, it may be involved in stabilization of nAChR complexes, export of the receptors from the ER due to interactions with trafficking proteins, or alterations in its turnover from the cell surface. For example, rapsyn binding to the α-helical domains corresponding to the inner vestibule of the α1β1γδ nAChR is required for surface expression of this receptor (Lee et al., 2009), and binding of UBXD4 to the cytoplasmic loop of α3 can interfere with its ubiquitination and, consequently, the number of α3-containing receptors at the cell surface (Rezvani et al., 2010). Thus, our studies point to two mechanisms mediated by specific residues in the inner vestibule, one leading to ion permeation changes within a single α3β4α5 receptor, and the other leading to increased surface expression of receptors by native β4.

Third, the studies presented here demonstrate that the MHb has a major influence in the control of nicotine consumption, extending previous studies of the role of the Hb in nicotine withdrawal and drug addiction (Jackson et al., 2008; Salas et al., 2004, 2009; Taraschenko et al., 2007) and, recently, in nicotine self-administration (Fowler et al., 2011). Although multiple interconnected brain regions, including the prefrontal cortex, VTA, thalamus, striatum, and amygdala are affected by chronic use of nicotine, the habenular system is emerging as an important station in pathways regulating the behavioral effects of nicotine (Changeux, 2010; De Biasi and Salas, 2008; Rose, 2007). The MHb projects mainly to the IPN, which, in turn, seems to inhibit the motivational response to nicotine intake. Thus, inactivation of the MHb and IPN both result in increased intake of nicotine (Fowler et al., 2011). Consistent with these studies, overexpression of β4 results in enhanced activity of the MHb, resulting in the opposing effect, e.g., aversion to nicotine. Reversal of nicotine aversion in Tabac mice overexpressing β4 is achieved by expression of the α5 D397N in MHb neurons. Similarly, α5 re-expression in the Hb of α5 KO mice normalizes their nicotine intake (Fowler et al., 2011). Taken together, these studies provide direct evidence that the MHb acts as a gatekeeper in the control of nicotine consumption and that the balanced contribution of β4 and α5 subunits is critical for this function. Further analyses of nAChR function in the habenulo-IPN tract and its associated circuitry will be required to fully understand the addictive properties of nicotine.

EXPERIMENTAL PROCEDURES

Two-Electrode Voltage-Clamp Recordings of *Xenopus* Oocytes

cDNA clones of the nAChR mouse subunits α3, α4, α5, β2, and β4 were subcloned into *pCS2+* plasmid for *Xenopus* oocyte expression and in vitro transcribed with T7 or SP6 RNA polymerases (mMESSAGE mMACHINE, Ambion, Austin, TX) as described in Ibañez-Tallon et al. (2004). β4 S435R, α5 D397N, and β2/β4 chimeras were cloned using a Mutagenesis Kit according to the manufacturer's instructions (Stratagene). Oocytes were surgically removed and prepared as described (Stürzebecher et al., 2010). Each oocyte was injected with 20 nl of a cRNA mix containing either 1 ng or 10 ng of one α and one β nAChR subunit in 1:1, 1:2, 1:3, 1:4, 1:5, 1:10, and 10:1 ratios. In a separate experiment, α5 WT and α5 D397N were coinjected at 1:10:1, 1:10:5, or 1:10:10 ratios (α3:β4:α5). Macroscopic currents were recorded between 2 and 5 days after injection with a GeneClamp 500B amplifier (Axon Instruments) using a two-electrode voltage clamp with active ground configuration. Electrodes (0.5–2 MΩ) were filled with 3M KCl. The extracellular recording solution contained 82.5 mM NaCl, 2 mM KCl, 1 mM $CaCl_2$, 1 mM $MgCl_2$, and 10 mM HEPES at pH 7.4. Nicotine-tartrate (Sigma-Aldrich) was prepared in extracellular solution at concentrations of 10 nM to 100 mM. Solutions were gravity fed with a flow rate of ~5 ml/min using a Bath Perfusion System valve controller (ALA-VM8, ALA Scientific Instruments). Data were acquired using pCLAMP9 software (Axon Instruments) and currents were sampled at 10 Hz. Membrane potential was clamped to −70 mV; only oocytes with leak currents <100 nA were used. Mean fold current increase was evaluated by dividing peak amplitudes of 5–10 single oocytes at each ratio by peak amplitudes at 1:1 ratio. All experiments were repeated twice. Dose-response curves were calculated relative to the maximal response to nicotine as described in Ibañez-Tallon et al. (2002).

Molecular Modeling

All models of pentameric α3α5β4 nAChR and single-residue variations were constructed with the program MODELER 9v7, using the structure of the nAChR from *T.marmorata* (PDB ID 2BG9) as a template for modeling. Energy equilibration and dynamics calculations were performed using GROMACS 3.3.3 applied to a pentameric α3α5β4 nAChR without the extracellular domain. After relaxation in an energy equilibration in OPLS-AA force field, the nAChR structures were compared.

Animals

Transgenic Tabac reporter mice were generated as described (Gong et al., 2003). Briefly, a BAC RP23-33606, containing the mouse *Chrnb4*, *Chrna3*, and *Chrna5* nicotinic receptor gene cluster, was recombined using a BAC engineering system by introducing an eGFP and a polyadenylation signal directly upstream of the coding sequence of the *Chrna3* gene. The modified BAC was injected into pronuclei of FVB/N fertilized oocytes, and hemizygous progeny was mated to Swiss Webster mice each generation thereafter. For stereotactic injection experiments and CPA, mice were backcrossed to C57BL/6 for six generations. All transgenic animals used for experiments were heterozygous. Mice were housed with ad libitum access to food and water in a room air conditioned at 22°C–23°C with a standard 12 hr light/dark cycle, with a maximum of five animals per cage. All procedures were in accordance with ethical guidelines laid down by the local governing body.

Western Blotting

Western blotting procedure was adapted from Grady et al. (2009). Briefly, the MHb was dissected from adult Tabac and WT mice (n = 3 per genotype), collected in 1 ml of lysis buffer (50 mM Na phosphate [pH 7.4], 1 M NaCl, 2 mM EDTA, 2 mM EGTA, and protease inhibitor cocktail), and immediately homogenized by passing the tissue 10 times through a syringe (27G). The homogenates were centrifuged for 30 min at 13,000 rpm and the pellet was resuspended in 500 μl of 50 mM Tris HCl [pH 7], 120 mM NaCl, 5 mM KCl, 1 mM MgCl2, and 2.5 mM $CaCl_2$ containing protease inhibitor cocktail. After addition of 2% Triton X-100, the membranes were extracted for 2 hr at 4°C. Supernatants were recovered after 10 min of centrifugation. Equal amounts of membrane extracts underwent SDS-PAGE and were transferred to PVDF membranes. Primary antibodies used were rabbit anti-beta4 (gift from Dr. Cecilia Gotti), mouse monoclonal (268) alpha5 mAb (Abcam, Cambridge, UK), or mouse monoclonal anti-α-tubulin (Sigma, St Louis, MO). After incubation with the appropriate HRP-conjugated secondary antibodies, peroxidase was detected using a chemiluminescent substrate (Pierce, Rockford, IL).

Brain Immunohistochemistry

Adult mice were injected with a lethal dose of ketamine and perfused transcardially with 4% paraformaldehyde in cold 0.1 M phosphate buffer (PB). Brains were fixed for 2–4 hr and transferred to 30% sucrose in PB. The next day, 40 μm coronal or sagittal sections were cut from a dry ice-cooled block on a sliding microtome (Leica) and kept in cryoprotectant (25% ethylene glycol, 25% glycerol, and 0.05 M PB) at −20°C until immunofluorescence labeling was performed. Selected brain sections were washed in PBS and pretreated with blocking buffer (0.3% Triton X-100 and 10% horse serum in phosphate buffered saline). All antibodies were diluted in PBT containing 0.3% Triton X-100 and 1% horse serum in PBS. Primary antibodies used were rabbit polyclonal anti-eGFP (Molecular Probes) and goat polyclonal anti-ChAT (Chemicon), both diluted 1:1000; rabbit polyclonal anti-calbindin D-28K (Swint) diluted 1:500; rabbit polyclonal anti-Substance P (Zymed) diluted 1:1000; or mouse monoclonal anti-Tyrosine hydroxylase (Sigma-Aldrich) diluted 1:2000 and incubated overnight at 4°C. Costaining with anti-eGFP was necessary to detect fluorescent signals in weak *Chrna3* expression areas (e.g., substantia nigra and VTA) and to visualize axonal/dendritic processes. Secondary antibodies used were goat anti-mouse IgG conjugated with Cy3 (Jackson) and donkey anti-goat IgG conjugated with Alexa Fluor 555 (Molecular Probes), both diluted 1:500 and incubated 2 hr at RT. Sections were washed, mounted on slides, and coverslipped in immu-mount (Thermo Scientific). Fluorescent signals were detected using a confocal laser scanning microscope (Leica SP5). A Biorevo fluorescent microscope (Keyence) was used for low-magnification pictures.

ISH

A mouse brain cDNA library was used to amplify bases 982–1382 from Chrnb4 and subcloned into the TOPO TA pCR2.1 vector (Invitrogen). After

linearization, antisense riboprobes were synthesized using T7 RNA polymerase and labeled with DIG according to the manufacturer's instructions (Roche Applied Science). ISH was performed on 20 μm coronal sections from WT and transgenic littermates as described before (Auer et al., 2010). The developing enzymatic color-reaction was stopped simultaneously in sections of WT and transgenic mice.

Acute Brain Slice Electrophysiological Recordings

Whole-cell patch-clamp recordings were made in coronal slices (250 μm) containing the MHb from WT and transgenic mice (P7–P14). Acute brain slices were cut with a vibratome (Microm HM 650 V) and kept in ice-cold oxygenated (95% O_2 and 5% CO_2) artificial cerebrospinal fluid (ACSF) containing (in mM) 125 NaCl, 2.5 KCl, 1.3 $MgCl_2$, 2 $CaCl_2$, 1.25 KH_2PO_4, 11 glucose, and 26 $NaHCO_3$ (pH 7.4, osmolarity 310) and allowed to recover for at least 1 hr in oxygenated ACSF at RT. The recording chamber was gravity fed with the same buffer. Hb neurons were visually identified with a microscope (Axioskop 2 FS plus) equipped with a digital camera (SPOT Insight). Patch electrodes were made from borosilicate glass (1B150F-4, World Precision Instruments, Inc.) with a microelectrode puller (P-97, Sutter Instrument, CO). The internal pipette solution contained (in mM) 130 KCl, 2 $MgCl_2$, 0.5 $CaCl_2$, 5 EGTA, and 10 HEPES (pH 7.3, osmolarity 280; resistance, 5–7 MΩ). Typical series resistance was 15–30 MΩ. Nicotine was locally applied (50 ms, 8–10 psi) at different concentrations (1–600 μM) with a pressure device (PR-10, ALA Scientific Instruments) connected to a focal perfusion system (VM4, ALA Scientific Instruments) controlled with a trigger interface (TIB 14S, HEKA). The pipette was moved within 15–20 μm of the recorded cell with a motorized micromanipulator (LN mini 25, control system SM-5, Luigs & Neumann) for drug application and retracted after the end of the puff to minimize desensitization. In current clamp, the pipette with nicotine was positioned 100 μm from the cell and the drug was applied for 3 s. Neurons showing spontaneous oscillations were not tested. Currents were recorded with a HEKA amplifier (EPC 10) using PatchMaster software (V2.20, HEKA), and were analyzed with FitMaster software (V2.3, HEKA). Membrane potential was held at −70 mV. Dose-response curves were calculated relative to the maximal response to nicotine (n = 3 cells per genotype).

Receptor Ligand Autoradiography

Adult brains were dissected and immediately embedded in O.C.T. compound (Sakura). Frozen tissues were cut at the cryostat (20 μm coronal sections), thaw mounted on ultrafrost microscope slides (Menzel Gläser), and stored at −80°C. For total [^{125}I]-epibatidine binding sites, sections of WT and transgenic littermates (n = 3 per genotype) were incubated with 200 pM [^{125}I]-epibatidine (NEN Perkin Elmer, Boston; specific activity 2200 Ci/mmole) in Tris 50 mM (pH 7.4) for 1 hr. For cytisine-resistant [^{125}I]-epibatidine binding sites, sections were first incubated with 25 mM Cytisine (Sigma, St Louis) in Tris 50 mM (pH 7.4) for 30 min, as described previously (Zoli et al., 1995). Quantification of binding was done with ImageJ (NIH).

Oral Nicotine Consumption: No-Choice Paradigm

WT (n = 5) and Tabac (n = 5) male mice were single housed in their home cages. Mice were provided with either nicotine or saccharin solutions as their sole source of fluid and bottles were weighed daily to measure nicotine intake. The volume of the drinking solution consumed per day was averaged for the period of consumption (3 days). Drinking solutions were: water, 2% saccharine in water (sweet water), 5 mM quinine (bitter water), or 100 μM nicotine in sweet water. Nicotine tartrate was dissolved in 0.9% sterile saline (all concentrations of nicotine refer to the free base form). The dose consumed was calculated as the milligrams of nicotine consumed per day considering the body weight of the mouse (mg/kg/d).

Oral Nicotine Consumption: Free-Choice Paradigm

Voluntary nicotine intake was assessed in adult male WT (n = 7) and Tabac (n = 6) mice, using the two-bottle assay as described before (Butt et al., 2005). Naive mice were presented with two bottles of water in the home cage for acclimatization to the new conditions for the first 3 days of testing. After this period, one of the bottles was filled with a nicotine solution (1 μg/ml) diluted in water. The intake of fluid from each bottle was measured daily for 3 days. The concentration of the nicotine solution was then increased and tested for another 3 days. In total, six different concentrations were tested consecutively (1, 5, 12.5, 25, 50, and 100 μg/ml). Percent of nicotine consumption was expressed as a ratio of the volume of nicotine solution consumed divided by the total fluid intake ([ml nicotine × 100%]/ml total).

CPA

The CPA apparatus used was a rectangular box composed of three distinct compartments separated by removable doors. The center compartment (10 × 20 × 10 cm) is gray with a polycarbonate smooth floor. The choice compartments (20 × 40 × 20 cm) have different visual and tactile cues. One choice compartment has black walls with a 0.75 cm stainless steel mesh floor. The other compartment has white walls with a 0.25 cm stainless steel mesh floor. Behavior of animals was videotaped and scored by a blind observer. In the preconditioning phase, on day 1, mice (8–12 weeks old) were allowed to explore the three compartments freely for 15 min. This preconditioning session was used to separate mice into groups with approximately equal biases for each side. None of the mice exhibited a strong preference for one side over the other. In the conditioning phase, during the following 3 days, two pairings per day were given at 4–5 hr apart. The doors between the compartments were closed so that animals were confined to one side or the other of the conditioning box for 15 min. In the morning the animals were given an i.p. saline injection prior to the placement in the chamber. In the afternoon, animals received a nicotine injection (i.p., 0.5 mg/kg) prior to the placement in the opposing chamber. In the preference test, on day 5, the doors between the compartments were opened again. Mice were placed in the central chamber and were allowed to move freely in the three chambers for 15 min. Time spent on each side was recorded.

Lentivirus Production

Recombinant lentiviral vectors were prepared using transient transfection of HEK293T cells. Briefly, 5 × 10^6 HEK293T cells were seeded on 24 × 10 cm cell-culture dishes precoated with poly-L-lysine (Sigma-Aldrich). The next day, the transfer vector plus the packaging vectors pLP1 and pLP2 (ViraPower System; Invitrogen) and the envelope vector pCMV-VSV-G (Addgene) were cotransfected with PEI transfection (Polyethylenimine MAX, Polysciences Inc.) into HEK293T cells. The transfection mix was prepared as follows (for one dish): 12 μg transfer plasmid, 6.5 μg pLP1, 3.5 μg pLP2, and 3.5 μg pCMV-VSV-G were added to 800 μl OptiMEM (GIBCO) and incubated at RT for 5 min. In the meanwhile, 51 μl PEI solution (1 mg/ml) was added to 800 μl OptiMEM in a separate tube. Both solutions were mixed and incubated at RT for 30 min. During the incubation time, the medium of the cells was changed to 5 ml OptiMEM per dish. Finally, 3 ml transfection mix was added to each dish. After 7–8 hr, the medium was replaced by 9 ml OptiMEM per dish, without addition of FBS. The virus-containing medium was harvested 40–45 hr after medium change, cleared by centrifugation at 2500 × g for 10 min at 4°C, and filtered through 0.45 μm filter units (Millipore). Virus concentration was carried out by ultracentrifugation in a Beckman Optima L-90K ultracentrifuge using a SW32 Ti rotor at 50,000 × g for 3 hr with a purification layer of 1 ml 20% sucrose (in dH_20) added to the bottom of the centrifuge tubes. Subsequently, the virus was resuspended in 50–100 μl 1× PBS, aliquoted, and stored at −70°C. The titer of concentrated lentivirus was determined by transducing 1 × 10^5 HEK293T cells per well in a 24-well cell-culture plate with limiting virus dilutions and quantification of GFP-positive cells by FACS analysis after 3 days. Titers of concentrated lentivirus were in the range of 5 × 10^8 – 2 × 10^9 TU ml^{-1}.

Stereotaxic Injections

Tabac mice, aged 8–13 weeks, were anesthetized with ketamine and xylazine (130 and 10 mg kg^{-1}) and placed in a Benchmark stereotaxic frame with a Cunningham mouse adaptor. One-half microliters of virus was injected bilaterally with a pulled glass pipette (flow rate 0.1 μl min^{-1}) into the MHb at the following coordinates: antero-posterior (from bregma): –1.4 mm and –1.75 mm; lateral: ± 0.36 mm; and dorso-ventral (from skull level): –2.7 mm and –2.72 mm. Behavioral experiments started 2 weeks after injections. Verification of the injection sites was done on brain sections immunostained with rabbit polyclonal anti-RFP (Molecular Probes) diluted 1:1000.

Statistical Analysis

Unpaired two-tailed Student's t tests were used for analyzing most of the data, except when two-way analysis of variance (ANOVA) or paired two-tailed Student's t tests are indicated. Results are presented as means ± SEM.

SUPPLEMENTAL INFORMATION

Supplemental Information for this article includes four figures, one table, and Supplemental Experimental Procedures and can be found with this article online at doi:10.1016/j.neuron.2011.04.013.

ACKNOWLEDGMENTS

We thank J. Xing (Rockefeller University, New York, NY), S. Wojtke, B. Kampfrath, and J. Reiche (MDC, Germany) for technical support. We also thank J. Stitzel for mouse nAChR clones (University of Colorado, Boulder, CO); W. Kummer (University of Giessen, Germany), G. Lewin (MDC, Germany), C. Birchmeier (MDC, Germany) and M. Andrade (MDC, Germany) for helpful discussions; A. Garratt (MDC, Germany) for providing the SP antibody; and F. Rathjen (MDC, Germany) for the CD28 antibody. This work was supported by the Helmholtz Association 31-002, the Sonderforschungsbereich SFB 665, the Deutsche Forschungsgemeinschaft DFG RA 424/5-1, MCB RAS, and RFBR.

Accepted: April 8, 2011
Published: May 11, 2011

REFERENCES

Amos, C.I., Gorlov, I.P., Dong, Q., Wu, X., Zhang, H., Lu, E.Y., Scheet, P., Greisinger, A.J., Mills, G.B., and Spitz, M.R. (2010a). Nicotinic acetylcholine receptor region on chromosome 15q25 and lung cancer risk among African Americans: a case-control study. J. Natl. Cancer Inst. *102*, 1199–1205.

Amos, C.I., Spitz, M.R., and Cinciripini, P. (2010b). Chipping away at the genetics of smoking behavior. Nat. Genet. *42*, 366–368.

Auer, S., Stürzebecher, A.S., Jüttner, R., Santos-Torres, J., Hanack, C., Frahm, S., Liehl, B., and Ibañez-Tallon, I. (2010). Silencing neurotransmission with membrane-tethered toxins. Nat. Methods *7*, 229–236.

Bacher, I., Wu, B., Shytle, D.R., and George, T.P. (2009). Mecamylamine - a nicotinic acetylcholine receptor antagonist with potential for the treatment of neuropsychiatric disorders. Expert Opin. Pharmacother. *10*, 2709–2721.

Bierut, L.J. (2010). Convergence of genetic findings for nicotine dependence and smoking related diseases with chromosome 15q24-25. Trends Pharmacol. Sci. *31*, 46–51.

Bierut, L.J., Stitzel, J.A., Wang, J.C., Hinrichs, A.L., Grucza, R.A., Xuei, X., Saccone, N.L., Saccone, S.F., Bertelsen, S., Fox, L., et al. (2008). Variants in nicotinic receptors and risk for nicotine dependence. Am. J. Psychiatry *165*, 1163–1171.

Bigger, C.B., Melnikova, I.N., and Gardner, P.D. (1997). Sp1 and Sp3 regulate expression of the neuronal nicotinic acetylcholine receptor beta4 subunit gene. J. Biol. Chem. *272*, 25976–25982.

Butt, C.M., King, N.M., Hutton, S.R., Collins, A.C., and Stitzel, J.A. (2005). Modulation of nicotine but not ethanol preference by the mouse Chrna4 A529T polymorphism. Behav. Neurosci. *119*, 26–37.

Carland, J.E., Cooper, M.A., Sugiharto, S., Jeong, H.J., Lewis, T.M., Barry, P.H., Peters, J.A., Lambert, J.J., and Moorhouse, A.J. (2009). Characterization of the effects of charged residues in the intracellular loop on ion permeation in alpha1 glycine receptor channels. J. Biol. Chem. *284*, 2023–2030.

Changeux, J.P. (2010). Nicotine addiction and nicotinic receptors: lessons from genetically modified mice. Nat. Rev. Neurosci. *11*, 389–401.

Dani, J.A., and Heinemann, S. (1996). Molecular and cellular aspects of nicotine abuse. Neuron *16*, 905–908.

De Biasi, M., and Salas, R. (2008). Influence of neuronal nicotinic receptors over nicotine addiction and withdrawal. Exp. Biol. Med. (Maywood) *233*, 917–929.

Dineley-Miller, K., and Patrick, J. (1992). Gene transcripts for the nicotinic acetylcholine receptor subunit, beta4, are distributed in multiple areas of the rat central nervous system. Brain Res. Mol. Brain Res. *16*, 339–344.

Flora, A., Schulz, R., Benfante, R., Battaglioli, E., Terzano, S., Clementi, F., and Fornasari, D. (2000). Transcriptional regulation of the human alpha5 nicotinic receptor subunit gene in neuronal and non-neuronal tissues. Eur. J. Pharmacol. *393*, 85–95.

Fowler, C.D., Lu, Q., Johnson, P.M., Marks, M.J., and Kenny, P.J. (2011). Habenular α5 nicotinic receptor subunit signalling controls nicotine intake. Nature *471*, 597–601.

Gahring, L.C., and Rogers, S.W. (2010). Nicotinic receptor subunit alpha5 modifies assembly, up-regulation, and response to pro-inflammatory cytokines. J. Biol. Chem. *285*, 26049–26057.

Glatt, A.R., Denton, K., and Boughter, J.D., Jr. (2009). Variation in nicotine consumption in inbred mice is not linked to orosensory ability. Chem. Senses *34*, 27–35.

Gong, S., Zheng, C., Doughty, M.L., Losos, K., Didkovsky, N., Schambra, U.B., Nowak, N.J., Joyner, A., Leblanc, G., Hatten, M.E., and Heintz, N. (2003). A gene expression atlas of the central nervous system based on bacterial artificial chromosomes. Nature *425*, 917–925.

Gotti, C., Clementi, F., Fornari, A., Gaimarri, A., Guiducci, S., Manfredi, I., Moretti, M., Pedrazzi, P., Pucci, L., and Zoli, M. (2009). Structural and functional diversity of native brain neuronal nicotinic receptors. Biochem. Pharmacol. *78*, 703–711.

Grady, S.R., Moretti, M., Zoli, M., Marks, M.J., Zanardi, A., Pucci, L., Clementi, F., and Gotti, C. (2009). Rodent habenulo-interpeduncular pathway expresses a large variety of uncommon nAChR subtypes, but only the alpha3beta4* and alpha3beta3beta4* subtypes mediate acetylcholine release. J. Neurosci. *29*, 2272–2282.

Ibañez-Tallon, I., Miwa, J.M., Wang, H.L., Adams, N.C., Crabtree, G.W., Sine, S.M., and Heintz, N. (2002). Novel modulation of neuronal nicotinic acetylcholine receptors by association with the endogenous prototoxin lynx1. Neuron *33*, 893–903.

Ibañez-Tallon, I., Wen, H., Miwa, J.M., Xing, J., Tekinay, A.B., Ono, F., Brehm, P., and Heintz, N. (2004). Tethering naturally occurring peptide toxins for cell-autonomous modulation of ion channels and receptors in vivo. Neuron *43*, 305–311.

Ikemoto, S., Qin, M., and Liu, Z.H. (2006). Primary reinforcing effects of nicotine are triggered from multiple regions both inside and outside the ventral tegmental area. J. Neurosci. *26*, 723–730.

Jackson, K.J., Martin, B.R., Changeux, J.P., and Damaj, M.I. (2008). Differential role of nicotinic acetylcholine receptor subunits in physical and affective nicotine withdrawal signs. J. Pharmacol. Exp. Ther. *325*, 302–312.

Kedmi, M., Beaudet, A.L., and Orr-Urtreger, A. (2004). Mice lacking neuronal nicotinic acetylcholine receptor beta4-subunit and mice lacking both alpha5- and beta4-subunits are highly resistant to nicotine-induced seizures. Physiol. Genomics *17*, 221–229.

Kelley, S.P., Dunlop, J.I., Kirkness, E.F., Lambert, J.J., and Peters, J.A. (2003). A cytoplasmic region determines single-channel conductance in 5-HT3 receptors. Nature *424*, 321–324.

Lee, Y., Rudell, J., and Ferns, M. (2009). Rapsyn interacts with the muscle acetylcholine receptor via α-helical domains in the alpha, beta, and epsilon subunit intracellular loops. Neuroscience *163*, 222–232.

Levitin, F., Weiss, M., Hahn, Y., Stern, O., Papke, R.L., Matusik, R., Nandana, S.R., Ziv, R., Pichinuk, E., Salame, S., et al. (2008). PATE gene clusters code for multiple, secreted TFP/Ly-6/uPAR proteins that are expressed in reproductive and neuron-rich tissues and possess neuromodulatory activity. J. Biol. Chem. *283*, 16928–16939.

Lu, B., Su, Y., Das, S., Wang, H., Wang, Y., Liu, J., and Ren, D. (2009). Peptide neurotransmitters activate a cation channel complex of NALCN and UNC-80. Nature *457*, 741–744.

Marks, M.J., Laverty, D.S., Whiteaker, P., Salminen, O., Grady, S.R., McIntosh, J.M., and Collins, A.C. (2010). John Daly's compound, epibatidine, facilitates identification of nicotinic receptor subtypes. J. Mol. Neurosci. *40*, 96–104.

Maskos, U. (2008). The cholinergic mesopontine tegmentum is a relatively neglected nicotinic master modulator of the dopaminergic system: relevance to drugs of abuse and pathology. Br. J. Pharmacol. *153* (*Suppl 1*), S438–S445.

Maskos, U., Molles, B.E., Pons, S., Besson, M., Guiard, B.P., Guilloux, J.P., Evrard, A., Cazala, P., Cormier, A., Mameli-Engvall, M., et al. (2005). Nicotine reinforcement and cognition restored by targeted expression of nicotinic receptors. Nature *436*, 103–107.

McGehee, D.S., and Role, L.W. (1995). Physiological diversity of nicotinic acetylcholine receptors expressed by vertebrate neurons. Annu. Rev. Physiol. *57*, 521–546.

McGehee, D.S., Heath, M.J., Gelber, S., Devay, P., and Role, L.W. (1995). Nicotine enhancement of fast excitatory synaptic transmission in CNS by presynaptic receptors. Science *269*, 1692–1696.

Medel, Y.F., and Gardner, P.D. (2007). Transcriptional repression by a conserved intronic sequence in the nicotinic receptor alpha3 subunit gene. J. Biol. Chem. *282*, 19062–19070.

Meliska, C.J., Bartke, A., McGlacken, G., and Jensen, R.A. (1995). Ethanol, nicotine, amphetamine, and aspartame consumption and preferences in C57BL/6 and DBA/2 mice. Pharmacol. Biochem. Behav. *50*, 619–626.

Nashmi, R., Dickinson, M.E., McKinney, S., Jareb, M., Labarca, C., Fraser, S.E., and Lester, H.A. (2003). Assembly of alpha4beta2 nicotinic acetylcholine receptors assessed with functional fluorescently labeled subunits: effects of localization, trafficking, and nicotine-induced upregulation in clonal mammalian cells and in cultured midbrain neurons. J. Neurosci. *23*, 11554–11567.

O'Dell, L.E., and Khroyan, T.V. (2009). Rodent models of nicotine reward: what do they tell us about tobacco abuse in humans? Pharmacol. Biochem. Behav. *91*, 481–488.

Perry, D.C., and Kellar, K.J. (1995). [3H]epibatidine labels nicotinic receptors in rat brain: an autoradiographic study. J. Pharmacol. Exp. Ther. *275*, 1030–1034.

Picciotto, M.R. (1998). Common aspects of the action of nicotine and other drugs of abuse. Drug Alcohol Depend. *51*, 165–172.

Quick, M.W., Ceballos, R.M., Kasten, M., McIntosh, J.M., and Lester, R.A. (1999). Alpha3beta4 subunit-containing nicotinic receptors dominate function in rat medial habenula neurons. Neuropharmacology *38*, 769–783.

Ren, X.Q., Cheng, S.B., Treuil, M.W., Mukherjee, J., Rao, J., Braunewell, K.H., Lindstrom, J.M., and Anand, R. (2005). Structural determinants of alpha4beta2 nicotinic acetylcholine receptor trafficking. J. Neurosci. *25*, 6676–6686.

Rezvani, K., Teng, Y., and De Biasi, M. (2010). The ubiquitin-proteasome system regulates the stability of neuronal nicotinic acetylcholine receptors. J. Mol. Neurosci. *40*, 177–184.

Robinson, S.F., Marks, M.J., and Collins, A.C. (1996). Inbred mouse strains vary in oral self-selection of nicotine. Psychopharmacology (Berl.) *124*, 332–339.

Rose, J.E. (2007). Multiple brain pathways and receptors underlying tobacco addiction. Biochem. Pharmacol. *74*, 1263–1270.

Saccone, N.L., Wang, J.C., Breslau, N., Johnson, E.O., Hatsukami, D., Saccone, S.F., Grucza, R.A., Sun, L., Duan, W., Budde, J., et al. (2009). The CHRNA5-CHRNA3-CHRNB4 nicotinic receptor subunit gene cluster affects risk for nicotine dependence in African-Americans and in European-Americans. Cancer Res. *69*, 6848–6856.

Salas, R., Pieri, F., and De Biasi, M. (2004). Decreased signs of nicotine withdrawal in mice null for the beta4 nicotinic acetylcholine receptor subunit. J. Neurosci. *24*, 10035–10039.

Salas, R., Sturm, R., Boulter, J., and De Biasi, M. (2009). Nicotinic receptors in the habenulo-interpeduncular system are necessary for nicotine withdrawal in mice. J. Neurosci. *29*, 3014–3018.

Scofield, M.D., Tapper, A.R., and Gardner, P.D. (2010). A transcriptional regulatory element critical for CHRNB4 promoter activity in vivo. Neuroscience *170*, 1056–1064.

Stürzebecher, A.S., Hu, J., Smith, E.S., Frahm, S., Santos-Torres, J., Kampfrath, B., Auer, S., Lewin, G.R., and Ibañez-Tallon, I. (2010). An in vivo tethered toxin approach for the cell-autonomous inactivation of voltage-gated sodium channel currents in nociceptors. J. Physiol. *588*, 1695–1707.

Tapper, A.R., McKinney, S.L., Nashmi, R., Schwarz, J., Deshpande, P., Labarca, C., Whiteaker, P., Marks, M.J., Collins, A.C., and Lester, H.A. (2004). Nicotine activation of alpha4* receptors: sufficient for reward, tolerance, and sensitization. Science *306*, 1029–1032.

Taraschenko, O.D., Shulan, J.M., Maisonneuve, I.M., and Glick, S.D. (2007). 18-MC acts in the medial habenula and interpeduncular nucleus to attenuate dopamine sensitization to morphine in the nucleus accumbens. Synapse *61*, 547–560.

Thorgeirsson, T.E., Geller, F., Sulem, P., Rafnar, T., Wiste, A., Magnusson, K.P., Manolescu, A., Thorleifsson, G., Stefansson, H., Ingason, A., et al. (2008). A variant associated with nicotine dependence, lung cancer and peripheral arterial disease. Nature *452*, 638–642.

Unwin, N. (2005). Refined structure of the nicotinic acetylcholine receptor at 4A resolution. J. Mol. Biol. *346*, 967–989.

Weiss, R.B., Baker, T.B., Cannon, D.S., von Niederhausern, A., Dunn, D.M., Matsunami, N., Singh, N.A., Baird, L., Coon, H., McMahon, W.M., et al. (2008). A candidate gene approach identifies the CHRNA5-A3-B4 region as a risk factor for age-dependent nicotine addiction. PLoS Genet. *4*, e1000125.

Whiting, P.J., and Lindstrom, J.M. (1988). Characterization of bovine and human neuronal nicotinic acetylcholine receptors using monoclonal antibodies. J. Neurosci. *8*, 3395–3404.

Xu, W., Gelber, S., Orr-Urtreger, A., Armstrong, D., Lewis, R.A., Ou, C.N., Patrick, J., Role, L., De Biasi, M., and Beaudet, A.L. (1999). Megacystis, mydriasis, and ion channel defect in mice lacking the alpha3 neuronal nicotinic acetylcholine receptor. Proc. Natl. Acad. Sci. USA *96*, 5746–5751.

Xu, X., Scott, M.M., and Deneris, E.S. (2006). Shared long-range regulatory elements coordinate expression of a gene cluster encoding nicotinic receptor heteromeric subtypes. Mol. Cell. Biol. *26*, 5636–5649.

Yang, K., Hu, J., Lucero, L., Liu, Q., Zheng, C., Zhen, X., Jin, G., Lukas, R.J., and Wu, J. (2009). Distinctive nicotinic acetylcholine receptor functional phenotypes of rat ventral tegmental area dopaminergic neurons. J. Physiol. *587*, 345–361.

Zoli, M., Le Novère, N., Hill, J.A., Jr., and Changeux, J.P. (1995). Developmental regulation of nicotinic ACh receptor subunit mRNAs in the rat central and peripheral nervous systems. J. Neurosci. *15*, 1912–1939.

Zoli, M., Léna, C., Picciotto, M.R., and Changeux, J.P. (1998). Identification of four classes of brain nicotinic receptors using beta2 mutant mice. J. Neurosci. *18*, 4461–4472.